Conference Paper

Towards Estimation and Correction of Wind Effects on a Quadrotor UAV

Author(s):
Schiano, Fabrizio; Alonso-Mora, Javier; Rudin, Konrad; Beardsley, Paul; Siegwart, Roland Y.; Sicilianok, Bruno

ETH Library

Towards Estimation and Correction of Wind Effects on a Quadrotor UAV

Fabrizio Schiano,* Javier Alonso-Mora,† Konrad Rudin,‡ Paul Beardsley,§ Roland Siegwart,¶ Bruno Siciliano‖

Abstract

In this paper the problem of estimation and correction of wind effects on a quadrotor UAV, without using wind sensors, is discussed. A large body of research addresses the effects of wind on a quadrotor, however most of them consider it only as a disturbance in their control loop and, for this reason, they solved the problem compensating for the wind with a powerful controller. The main part of this paper is related to the modeling of wind on a quadrotor and to the wind tunnel tests performed at the IFD wind tunnel of ETH Zurich. The approach presented can be used as a starting point for future works. The results obtained in the wind tunnel are really promising for the formulation of a complete aerodynamic model of the quadrotor that has been missing until now.

1 Introduction

Quadrotors are becoming really popular in recent years both for their field of application and, for the multidisciplinarity applications that they offer (i.e. Mechanics, Electronics, Control Theory, Aerodynamics and so on). They are useful for their high capability of Vertical Take Off and Landing (VTOL), high controllability and maneuverability. Moreover, unlike most fixed wing UAVs, the quadrotors are able to hover in a certain position. For all these reasons, they are more suitable to be used for tasks such as of mapping and 3D- image-reconstruction of a specific area. Moreover, they also provide good capabilities in building costruction [1], monitoring of public places, avoidance of terroristic attacks, in search and rescue missions after an environmental disaster and entertainment [2].

The goal of this work is to estimate and correct wind effects on a quadrotor [3] without adding wind sensors on it (because of the high cost and difficulty to install them on a quadrotor).

In most of the cases reported in literature, wind is not considered explicitly, and so, the controller uses it just as a disturbance to reject. In some cases it would be useful to estimate wind in order to have a wind measurement to add to the control loop and to save money for buying a wind sensor or to have a *quadrotor anemometer* wherever needed.

This paper is organized as follows. First, the model of the quadrotor, focusing on the role of wind into the equations of the model, will be analyzed. Then, a short overview of the platform used for the real experiments is presented. The control strategy used to control the quadrotor will then be presented and finally, the approach to estimate wind giving a main focus to the tests performed in the wind tunnel to identify some of the parameters belonging to the aerodynamic model of the quadrotor will be introduced.

2 Model and Controller of the Quadrotor

2.1 Model of the Quadrotor

The main equations of the model of the quadrotor come from [4] and [5]. The starting point for their formulation is the application of the Newton-Euler approach[1] to rigid body dynamics equations. Furthermore, the modeling assumptions are reported below:

1. The input of the system is the speed of the rotors.

2. The outputs of the system are its position and attitude.

3. The CoG and the body frame origin are assumed to coincide.

4. The propellers are supposed to be rigid.

The rigid body dynamics equations can be split into two parts: force equations (Equation 1) and moment equations (Equation 2).

$$m\mathbf{I}_{3\times3}\dot{\mathbf{v}} + \omega \times m\mathbf{v} = \mathbf{F} \tag{1}$$

*Fabrizio Schiano received both his B.Sc and M.Sc in Automation Engineering from the University of Naples Federico II. He is a researcher at Zentrum für Telematik (Gerbrunn, Germany) since July 2013. `fabrizio.schiano@gmail.com`

†Javier Alonso-Mora is a researcher at the Autonomous Systems Lab at ETH Zurich and Disney Research Zurich `jalonso@disneyresearch.com`

‡Konrad Rudin is a Ph.D candidate at the Autonomous Systems Lab at ETH Zurich `konrad.rudin@mavt.ethz.ch`

§Paul Beardsley is Principal Research Scientist at Disney Research Zurich. `pab@disneyresearch.com`

¶Roland Siegwart is full professor for autonomous systems at ETH Zurich and Director of the Autonomous Systems Lab at ETH Zurich. `rsiegwart@ethz.ch`

‖Bruno Siciliano is full professor of Control and Robotics, and Director of the PRISMA Lab at University of Naples Federico II. `siciliano@unina.it`

[1]The Newton-Euler approach is based on the equilibrium of forces and moments acting on the object analysis.

$$\mathbf{J}\dot{\omega} + \omega \times J\omega = \tau \qquad (2)$$

With:

m: Body mass

$\mathbf{I}_{3\times3}$: Identity Matrix

ω: Body angular speed

F: External force

$\mathbf{J} \in \mathbb{R}^{3\times3}$: The Inertia matrix

$\mathbf{v}$: Body linear speed

τ: External moment

These terms have the following expression:

$$\mathbf{I}_{3\times3} = \begin{bmatrix} 1 & 0 & 0 \\ 0 & 1 & 0 \\ 0 & 0 & 1 \end{bmatrix} \qquad \omega = \begin{bmatrix} p \\ q \\ r \end{bmatrix} \qquad \mathbf{F} = \begin{bmatrix} F_x \\ F_y \\ F_z \end{bmatrix} \qquad (3)$$

$$\mathbf{J} = \begin{bmatrix} J_{xx} & 0 & 0 \\ 0 & J_{yy} & 0 \\ 0 & 0 & J_{zz} \end{bmatrix} \qquad \mathbf{v} = \begin{bmatrix} u \\ v \\ w \end{bmatrix} \qquad \tau = \begin{bmatrix} \tau_x \\ \tau_y \\ \tau_z \end{bmatrix} \qquad (4)$$

Particular attention was given to the inertia matrix $\mathbf{J}$ and for this reason a CAD model of the quadrotor, shown in Figure 1, was designed.
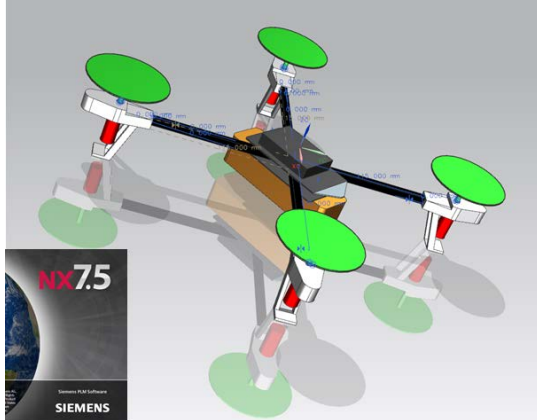

Figure 1: CAD Model of the Quadrotor

$$\mathbf{J} = \begin{bmatrix} J_{xx} & J_{xy} & J_{xz} \\ J_{yx} & J_{yy} & J_{yz} \\ J_{zx} & J_{zy} & J_{zz} \end{bmatrix} \qquad (5)$$

The results from the CAD software made clear that the products of inertia can be neglected. As expected, the terms on the diagonal are different from each other because the real quadrotor is not symmetric with respect to x, y and z. Therefore, the inertia matrix used in the model is:

$$\mathbf{J} = \begin{bmatrix} 1.79e{-}3 & 0 & 0 \\ 0 & 1.95e{-}3 & 0 \\ 0 & 0 & 3.56e{-}3 \end{bmatrix} [Kg \cdot m^2] \qquad (6)$$

Equation 1 and 2 can be written in a compact form:

$$\begin{bmatrix} m\,\mathbf{I}_{3\times3} & 0 \\ 0 & \mathbf{J} \end{bmatrix}\begin{bmatrix} \dot{\mathbf{v}} \\ \dot{\omega} \end{bmatrix}\begin{bmatrix} \omega \times m\,\mathbf{v} \\ \omega \times \mathbf{J}\,\mathbf{v} \end{bmatrix} = \begin{bmatrix} \mathbf{F} \\ \tau \end{bmatrix} \qquad (7)$$

Introducing the *Euler angles*:

$$[\phi \ \ \theta \ \ \psi \ ]^T \qquad (8)$$

their time derivative will be related to the angular rates of the quadrotor in the inertial frame through the following expression:

$$[\dot{\phi} \ \ \dot{\theta} \ \ \dot{\psi}]^T = \mathbf{M}^{-1} [\omega_{x_i} \ \ \omega_{y_i} \ \ \omega_{z_i}]^T \qquad (9)$$

where the M matrix is:

$$\mathbf{M} = \begin{bmatrix} \frac{c\psi}{c\theta} & \frac{s\psi}{c\theta} & 0 \\ -s\psi & c\psi & 0 \\ 0 & 0 & 1 \end{bmatrix} \qquad (10)$$

In order to have the relation between the time derivative of the Euler angles and the angular rates of the quadrotor in the body frame the following equation was used:

$$[\dot{\phi} \ \ \dot{\theta} \ \ \dot{\psi}]^T = \mathbf{M}^{-1} [\omega_{x_b} \ \ \omega_{y_b} \ \ \omega_{z_b}]^T \qquad (11)$$

where the $\mathbf{R}_B^I$ matrix is the rotation matrix which expresses the rotation to go from the body frame to the inertial frame:

$$\mathbf{R}_B^I \begin{bmatrix} c\psi c\theta & c\psi s\theta s\phi - s\psi c\phi & c\psi s\theta c\phi + s\psi s\phi \\ s\psi c\theta & s\psi s\theta s\phi + c\psi c\phi & s\psi s\theta c\phi - c\psi s\phi \\ -s\theta & c\theta s\phi & c\theta c\phi \end{bmatrix} \qquad (12)$$

where $c\psi = \cos(\psi)$, $s\psi = \sin(\psi)$.

In the same way, it is possible to get the linear velocities in the body frame from the linear velocities in the inertial frame:

$$[\dot{x}_b \ \ \dot{y}_b \ \ \dot{z}_b]^T = (\mathbf{R}_B^I)^{-1} [\dot{x}_i \ \ \dot{y}_i \ \ \dot{z}_i]^T \qquad (13)$$

The next step consists of the characterization of Equation 7 for the quadrotor. It is easier to look separately at the force and moment equations.

The model of the quadrotor was obtained by considering that it is near to the hover condition. In this case, the main forces and moments come from the propellers. Moreover, from Equation 10 and 12, it is clear that the $\mathbf{M}$ and $\mathbf{R}_B^I$ matrices become:

$$\mathbf{M}|_{(\phi,\theta,\psi=0)} = \mathbf{R}_B^I|_{(\phi,\theta,\psi=0)} = \begin{bmatrix} 1 & 0 & 0 \\ 0 & 1 & 0 \\ 0 & 0 & 1 \end{bmatrix} \qquad (14)$$

$$\implies [\dot{\phi} \ \ \dot{\theta} \ \ \dot{\psi}]^T = [\omega_{x_i} \ \ \omega_{y_i} \ \ \omega_{z_i}]^T = [\omega_{x_b} \ \ \omega_{y_b} \ \ \omega_{z_b}]^T \qquad (15)$$

2.2 Force Equations

The thrust generated by a propeller is proportional to the square of its rotational speed [6]. For the purposes of this work the thrust generated by a propeller will be addressed just as a term proportional to the square of its rotational speed:

$$T_i = b \, \Omega_i^2; \qquad b : thrust \; constant \qquad (16)$$

The equilibrium of the forces can be written as follows:

$$\begin{bmatrix} \ddot{x}_i \\ \ddot{y}_i \\ \ddot{z}_i \end{bmatrix} = - \begin{bmatrix} \omega_{x_b} \\ \omega_{y_b} \\ \omega_{z_b} \end{bmatrix} \times \begin{bmatrix} \dot{x}_i \\ \dot{y}_i \\ \dot{z}_i \end{bmatrix} + g \begin{bmatrix} 0 \\ 0 \\ 1 \end{bmatrix} + \frac{\mathbf{F}_{wI}}{m}$$

$$- \frac{T_1 + T_2 + T_3 + T_4}{m} \mathbf{R}_B^I \begin{bmatrix} 0 \\ 0 \\ 1 \end{bmatrix} \qquad (17)$$

where $\mathbf{F}_{wI}$ represents the disturbance force due to uncontrollable factors such as wind. It is important to highlight that this term represents force disturbances related to wind only under the assumption that other force disturbances can be neglected.

2.3 Moment Equations

The drag moment generated by a propeller is proportional to the square of its rotational speed [6]. The thrust and the drag moment generated by a propeller will be considered just as a term proportional to the square of its rotational speed:

$$D_i = d \, \Omega_i^2; \qquad d : drag \; constant \qquad (18)$$

The equilibrium of the moments can be written as follows:

$$\begin{bmatrix} \dot{\omega}_{x_b} \\ \dot{\omega}_{y_b} \\ \dot{\omega}_{z_b} \end{bmatrix} = -\mathbf{J}^{-1} \, \omega \times \mathbf{J} \begin{bmatrix} \omega_{x_b} \\ \omega_{y_b} \\ \omega_{z_b} \end{bmatrix}$$

$$+ \mathbf{J}^{-1} \begin{bmatrix} L(T_4 - T_2) \\ L(T_1 - T_3) \\ D_1 - D_2 + D_3 - D_4 \end{bmatrix} - \mathbf{J}^{-1} \, \tau_{\mathbf{d}} \qquad (19)$$

where τ_d represents the disturbance torque due to uncontrollable factors such as wind. As for the force equations, this term represents moment disturbances related to wind only under the assumption that other moment disturbances can be neglected. For convenience, the following effects were neglected:

- Gyrospcopic moments caused by the combination of rotations of the four propellers and vehicle frame.

- Friction torque due to rotational motion [7].

3 CONTROLLER

3.1 LQR Controller

The controller used for the quadrotor is shown in Figure 2 can be split into a *Position Controller* (off-board) and an *Attitude Controller* (on-board).
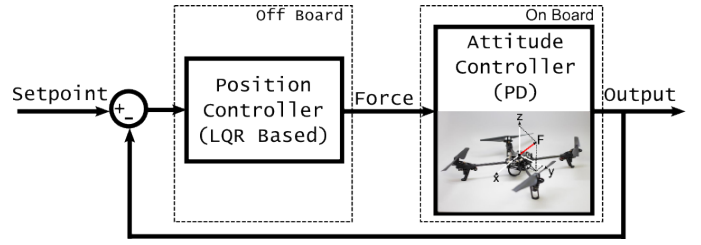

Figure 2: Scheme of the overall control structure

The *Position Controller* is a Linear Quadratic Regulator (LQR) giving the quadrotor a force vector that is interpreted on-board.

The *Attitude Controller* is a PD controller running at 250 Hz. The LQR control law is based on an algorithm which minimizes a cost function containing weighting factors chosen ad-hoc. It consists of an automated way to find the optimal state-feedback controller. The LQR controller is not the main goal of this work and, for this reason, only a short overview of it is provided. The goal of the LQR is to find the feedback control law $\mathbf{u}^*(t)$ which minimizes the quadratic cost function:

$$\mathbf{J}(\mathbf{x}(t), \mathbf{u}(t)) = \int_0^\infty \mathbf{x}(t)^T \mathbf{Q} \, \mathbf{x}(t) + \mathbf{u}(t)^T \mathbf{R} \, \mathbf{u}(t) \, dt \qquad (20)$$

This is represented by:

$$\mathbf{u}^*(t) = -\mathbf{K}_{LQR} \mathbf{x}(t) \qquad (21)$$

where $\mathbf{K}_{LQR}$ is given by:

$$\mathbf{K}_{LQR} = \mathbf{R}^{-1} \mathbf{B}^T \mathbf{P}(t) \qquad (22)$$

where $\mathbf{P}$ is the solution of the continuous time *Algebraic Riccati Equation*(ARE) and *Q,R* are:

$$Q = Q^T, \; Q \geq 0; \; R = R^T, \; R > 0. \qquad (23)$$

It must be underlined that the LQR itself is not able to reject constant disturbances and, for this reason, in the following paragraph a solution to deal with this problem is presented.

3.2 LQRI Controller

One way to solve the problem previously mentioned is to add an integral part to the LQR controller implementing a so-called *LQRI* controller. The LQRI is based on the extension of the system's state vector with the integral of the output as shown in Figure 3. It is important to highlight why the constant disturbances are of interest. The two main reasons were:

- The mass of the quadrotor can change because different batteries, which have different weights, were used.

- The input given to the motors was an integer number $\delta \in [0 - 500]$ but, to link this δ to the thrust $\mathbf{T}$ generated
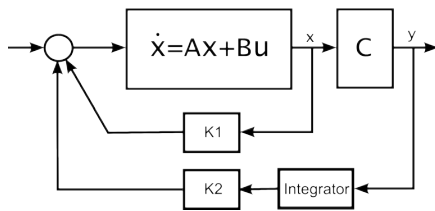
Figure 3: LQRI Controller Scheme

by the propellers, it was used a *thrust function* identified at the beginning of the PixHawk project [8]. It was noticed that the mapping between the δ and the **T** was wrong.

In control theory, in both cases described before, the result is a constant disturbance.

3.3 LQR-LQRI Results

In Figure 4-5, some results about the performances of the LQR and of the LQRI controller are showed. Both figures deal with the following test: in the interval $10-40s$ a setpoint at an altitude of $1\,m$ was given to the quadrotor, followed by a setpoint of $1.5\,m$ in the interval $40-60s$, then again $1\,m$ for a few seconds and finally the *land* command was given to the quadrotor.

From Figures 4-5 it can be observed that with the LQR controller there is a constant error of about $0.8\,m$, a big error which can not be accepted. An alternative to the LQRI controller could be to insert into the model of the quadrotor a fake mass which has to be changed every time there is a modification in the mass of the quadrotor, but this is not the best and the most formal solution. To solve this problem and to get rid of constant disturbances, the LQRI was implemented. Furthermore, several tests were performed to identify a better thrust function[2].
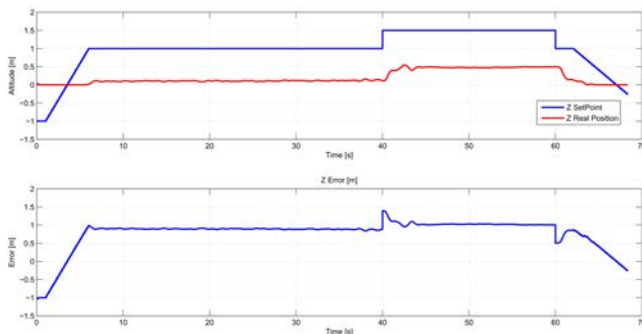
The improvements given from the LQRI are underlined in Figure 5. In the graph it can be observed that with the LQRI an error of about $0.015\,m$ was achieved. It can be considered a good performance for the purposes of the study.

4 THE PLATFORM

The quadrotor used in this work is shown in Figure 6. It has the frame of the Parrot AR Drone 2.0 [9], with the same propellers, motors and motor controllers. The Parrot frame was selected for its low cost, good strength, and low weight (400g ca.). The main electronics related to the quadrotor are composed of:

1 PX4FMU Autopilot / Flight Management Unit.

2 PX4IOAR ARDrone Carrier/Adapter.

3 RF Laird Board Base Station (connected to the Real-Time PC).

4 RF Laird Board Module (connected to the quadrotor).

The quadrotor's power supply is represented by 3-cell LiPo batteries with 1800 mAh[3] and a voltage of 11.1V.
The position and the attitude of the quadrotor were measured through the Vicon Motion Capture System. The main characteristics of this system of infrared cameras are:

- Speed: the system can be run at or below 375 Hz (in our experiments, a frequency of 200-250 Hz was used).

- Precision: experimental tests show that the deviations of position estimates for single static markers are of the order of 50 microns which is well beyond the requirements for a good flight.

- Robustness: using the VICON Tracker software, tracking of objects such as quadrotors is rarely lost, even during extreme situations such as fast maneuvers (speeds of $3.0m/s$, accelerations of $12m/s^2$ and angular speeds of 800 deg/s [10]).
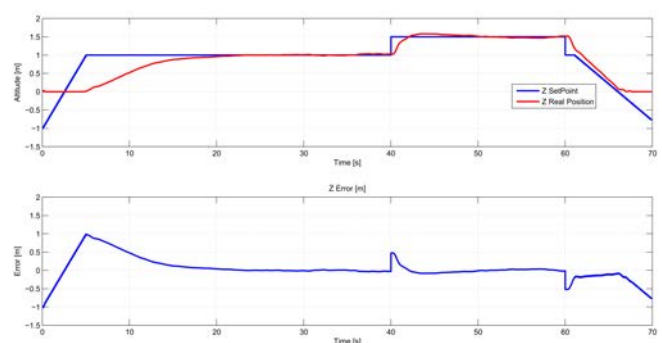

Figure 4: LQR Results in an experiment of different Altitudes

Figure 5: LQRI Results in an experiment of different Altitudes

---

[2]The thrust function relates the input given to the motors to the effective thrust generated by them.

[3]In this project both 1800 mAh and 2200 mAh batteries were used.

Figure 6: The quadrotor used in the tests with a focus on the VICON passive markers used to track it through the VICON system.

On the other hand, the software used for this work was mainly based on Matlab/Simulink® and the main feature of the MathWorks Software useful for the project was the $Real-TimeWindowsTarget^{TM}$ [11]. This toolbox provides a real-time engine for executing Simulink models on a Microsoft Windows® PC and blocks to interface an application to a wide range of I/O boards. It allows to create and control a real-time system for rapid prototyping and hardware-in-the-loop simulation.

The communication link to and from the quadrotor was established thanks to RF communication through:

1 *RF Laird Board Base Station*: used as a TX/RX on the PC-Side (shown in Figure 7.a).

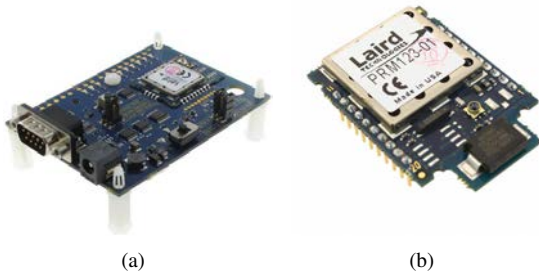2 *RF Laird Module*: used as a TX/RX on the quadrotor-Side (shown in Figure 7.b).

(a)　　　　　　　　(b)

Figure 7: Communication: (a) RF Laird board Base Station and (b) RF Laird Module

5　Wind Tunnel Experiments

The main reasons to perform such experiments in the wind tunnel are listed below:

1 Identification of $c_D A$ coefficient, where c_D is the drag coefficient of the quadrotor and A is the area of the quadrotor interested by the flow of the wind [m^2].

2 Identification of $c_L A$ coefficient, where c_L is the lift coefficient of the quadrotor.

3 Identification of wind's influence on the magnitude of the Thrust Vector **T**.

The area A of the quadrotor interested by the flow of the wind is not easy to compute due to its irregular shape and for this reason in this work it was not separated respectively from the drag (c_D) and lift (c_L) coefficients. The identification performed, as previously explained, is of the whole terms $c_D A$ and $c_L A$.

The wind tunnel used, shown in Figure 8, is located at the facilities of the Institute of Fluid Dynamics (IFD) of ETH. In that department, there are three different wind tunnels and, for this work, the largest one was chosen.

Figure 8: Wind Tunnel of IFD-ETH (Image courtesy of IFD-ETH) [12]

To identify the coefficients listed before, it was needed to measure, during the experiments, the three forces acting on the quadrotor. For this purpose, a six-axis force balance was used (ATI Mini40-E Transducer in Figure 9.a).

In this Section, the different kinds of experiments performed in the wind tunnel will be described[4]. In particular, the experiments can be divided in three categories:

1 Yaw Experiments[5].

2 Pitch Experiments[6].

3 Thrust Experiments.

Both yaw and pitch experiments were performed with the propellers left loose, while the thrust experiments were performed changing the input to the motors.

The final result of the fixation of the quadrotor in the wind tunnel is showed in Figure 12 and a detailed view of the assembly between the force sensor and the two adapter plates is showed in Figure 9.b.

---

[4]The choice of such experiments is driven by time, money and the wind tunnel waiting list.

[5]The yaw experiments were performed at these angles: $[-90°, -75°, -60°, -45°, -30°, -15°, 0°, 15°, 30°, 45°, 60°, 75°, 90°]$. The signs of the angles are chosen according to Figure 10.

[6]The pitch experiments were performed at these angles: $[-10°, 0°, 10°, 20°, 30°]$. The signs of the angles are chosen according to Figure 10.
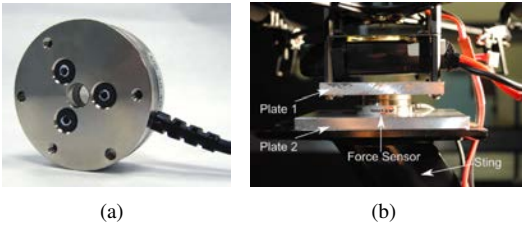
(a)   (b)

Figure 9: (a)Force sensor ATI Mini40-E and (b)a detailed view of the fixation of the quadrotor on the force sensor
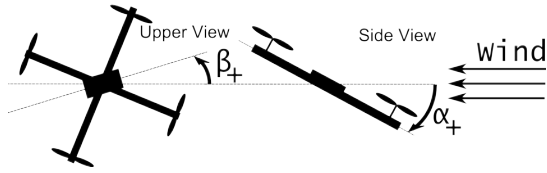

Figure 10: Positive Yaw and Pitch angles

All the experiments were performed at three different wind speeds:

$$\text{Wind Speeds} = [4.7, 9.6, 12.9] \ m/s$$

The wind tunnel has an integrated wind sensor (Figure 11.a) that is based on the pressure measurement on a sensitive surface, but this sensor is not fully reliable at such low speeds[7].

For this reason, to have a double check of this measurement, a hot wire anemometer TMA-21HW was used (Figure 11.b). The main equations, on which the tests are based, are the following:

$$\begin{cases} F_{mx} = -D\cos\alpha\cos\beta - (L - mg)\sin\alpha\cos\beta \\ F_{my} = -D\cos\alpha\sin\beta - (L - mg)\sin\alpha\sin\beta \\ F_{mz} = -D\sin\alpha + (L - mg)\cos\alpha + |\mathbf{T}| \end{cases} \quad (24)$$

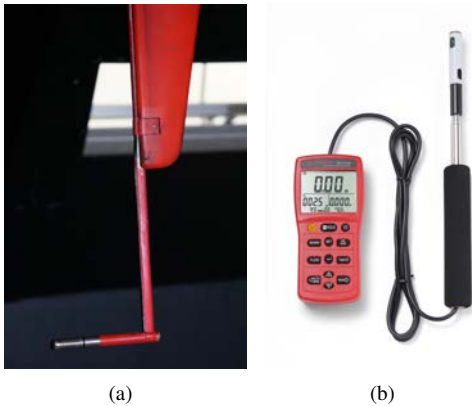

(a)   (b)

Figure 11: Wind Sensors: (a) Wind tunnel pressure sensor; (b) Hot wire anemometer TMA-21HW

.

[7]This wind tunnel is mostly used at its maximum wind speeds, which are around $50 \ m/s$.

Where:
F_{mx}: measured force on the x axis of the force sensor [N]
F_{my}: measured force on the y axis of the force sensor [N]
F_{mz}: measured force on the z axis of the force sensor [N]
$\mathbf{T}$: Thrust vector [N]
D: Magnitude of Drag Force [N]
L: Magnitude of Lift Force [N]
α and β are two angles which give the orientation of the wind with respect to the body axes of the quadrotor. In the wind tunnel, the quadrotor is fixed and the wind is always blowing in the same horizontal direction. For this reason, the angles α and β of Equation 24 in the wind tunnel coincide with the pitch and yaw angles of the quadrotor.

It is assumed that the *Drag Force* has the following expression (according to the Rayleigh equation):

$$\mathbf{D} = \frac{1}{2}c_D A\rho V_w \mathbf{V}_w \quad (25)$$

where:
V_w: Wind Speed [m/s]
$\mathbf{V}_w$ is a unit vector giving the wind direction.

From the previous equation, it is clear that the *drag force* is a vector with magnitude |$\mathbf{D}$| and with a direction that is always in the same direction of the wind vector $\mathbf{V}_w$.

Similarly to the Drag Force, it was assumed that the *Lift Force* has the following expression (according to the Rayleigh equation):

$$\mathbf{L} = \frac{1}{2}c_L A\rho V_w \mathbf{V}_{w\perp} \quad (26)$$

where $\mathbf{V}_{w\perp}$ is a unit vector perpendicular to the wind direction. From Equation 24, it follows that the identification of the $\mathbf{L}$ will be done through the observation of experiments at different pitch angles because it is related to the $\sin\alpha$.

The force sensor was not compensated for the force of gravity and for this reason that force is present in the previous equations.
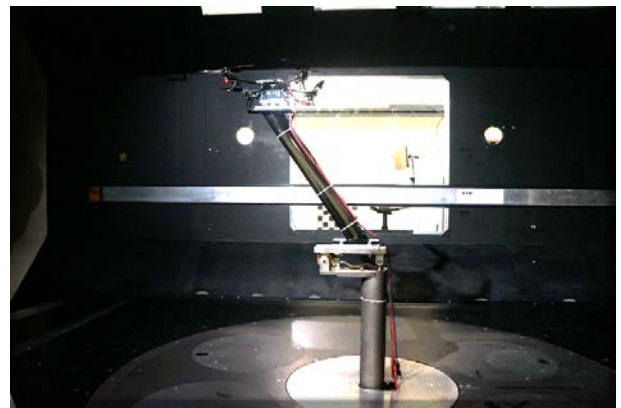

Figure 12: Quadrotor fixed in the wind tunnel

5.1 Yaw Experiments

While planning experiments in the wind tunnel,the approximation of the quadrotor to a cylinder sounded reasonable but, the tests proved that this is not true. From Figure 13, it is possible to see that the forces on the $x - y$ axis change according to the yaw angle variations and, for this reason, it is certain that there is a function that relates the $c_D A$ to the yaw angle.
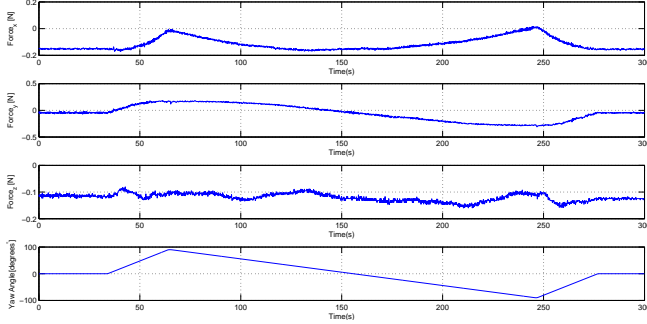

Figure 13: Forces in xyz with a $V_w = 4.7\,m/s$ and yaw variation

To analyze the data with $\alpha = 0$ and $\mathbf{T} = 0$, the system of Equations 24 becomes:

$$\begin{cases} F_{mx} = -D\cos\beta \\ F_{my} = -D\sin\beta \\ F_{mz} = (L - mg) \end{cases} \quad (27)$$

To have the drag force, only the 1st and the 2nd equation can be used. Solving the previous system of equations with respect to D will give:

$$D = \sqrt{F_{mx}^2 + F_{my}^2} \quad (28)$$

If the previous equation is applied to data corresponding to yaw angles $\beta \in [-90°, 90°]$, the result will be the $D(\beta)|_{\beta \in [-90°, 90°]}$ drag force as a function of β. From the drag force, it is easy to extract the $c_D A$ coeffient that will be, of course, a function of β:

$$c_D A = \frac{2D}{\rho V_w^2} \quad (29)$$

applying this inversion to the previous data of the drag force, the *drag coefficient function* $c_D A(\beta)$ showed in Figure 14[8] for different wind speeds will be deduced.
Figure 14 draws attention to the poor reliability of the lowest wind speed experiment (4.7 m/s). This is due to the fact that the wind tunnel is usually used at high wind speeds because at such low wind speeds it can not ensure a laminar flow of the

---

[8]The density of the air ρ was accurately measured in the wind tunnel and on the day of the experiments was of 1.1283 Kg/m^3

wind. Indeed it is clear from Figure 14 that measurements at 9.6 and 12.9 m/s are the most reliable. They are quite similiar to each other and they do not present the problem of different $c_D A(\beta)$ for $\beta = \pm 90°$.
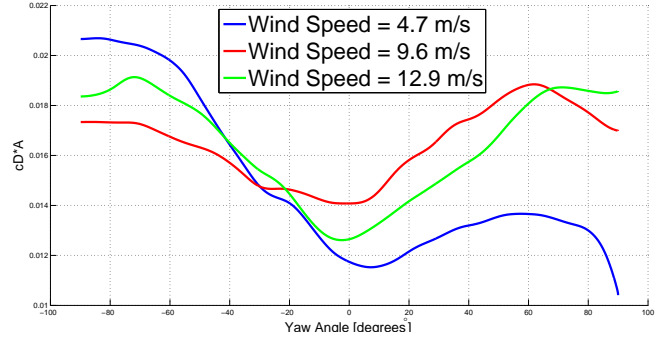

Figure 14: $c_D A(\beta)$ at different wind speeds

5.2 Pitch Experiments

In the pitch experiments, the yaw angle (β) is always equal to $0°$. For this reason, the system of Equations 24 will become:

$$\begin{cases} F_{mx} = -D\cos\alpha - (L - mg)\sin\alpha \\ F_{my} = 0 \\ F_{mz} = -D\sin\alpha + (L - mg)\cos\alpha + |\mathbf{T}| \end{cases} \quad (30)$$

The pitch angles chosen for the experiments were the following: [-10°,0°,10°,20°,30°]. Analyzing the data of the pitch experiments, the Tables 1-2 were obtained.

From the results in Tables 1-2, it can be assumed that the $c_D A$ is a function only of the yaw angle (β) because it seems that this coefficient is not changing a lot as in the yaw experiments. This is a strong assumption and it should be validated with other experiments.

Another result from Tables 1-2 is that the $c_L A$ is really small compared to the drag effect.

5.3 Thrust Experiments

Another category of experiments performed during this work were the thrust experiments, mainly for two reasons:

1 Identification of the *thrust function*: the function which relates the input δ given to the motors to the total thrust $|\mathbf{T}|$ they generate was refined.

2 Identification of the wind influence on the thrust vector: it was clear that the wind has an influence both on the direction and on the magnitude of the thrust vector $\mathbf{T}$.

Table 1: $c_D A, c_L A$ at wind speed of 9.6 m/s and different pitch angles ($\beta = 0°$ and $\mathbf{T} = 0$).

Pitch Angle (α)	$\mathbf{V_w = 9.6\,m/s}$	
−10°	$c_D A = 0.0143$	$c_L A = 0.0054$
0°	$c_D A = 0.0142$	$c_L A = 0.0017$
10°	$c_D A = 0.0119$	$c_L A = -0.0028$
20°	$c_D A = 0.0139$	$c_L A = 0.0018$
30°	$c_D A = 0.0119$	$c_L A = 0.0033$

Table 2: $c_D A, c_L A$ at wind speed of 12.9 m/s and different pitch angles ($\beta = 0°$ and $\mathbf{T} = 0$).

Pitch Angle (α)	$\mathbf{V_w = 12.9\,m/s}$	
−10°	$c_D A = 0.0144$	$c_L A = 0.0052$
0°	$c_D A = 0.0118$	$c_L A = 0.0048$
10°	$c_D A = 0.0146$	$c_L A = 0.0033$
20°	$c_D A = 0.0140$	$c_L A = 0.0002$
30°	$c_D A = 0.0141$	$c_L A = 0.0008$

As previously mentioned, the main result of the experiments performed in the wind tunnel was the identification of some terms of the aerodynamic model of the quadrotor such as $c_D A$ and $c_L A$. In this way, it was possible to simulate the behavior of the quadrotor in case of wind in a more realistic way. After the identification of some terms of the aerodynamic model of the quadrotor such as $c_D A$ and $c_L A$, it was possible to add wind into the simulator in a reasonable way. To do that, one choice is to add wind as a velocity vector with three components.

6 CONCLUSIONS AND FUTURE WORKS

In this work an approach to estimate wind and its influence on the state of a quadrotor was showed. During the work, an LQR/LQRI controller was implemented in order to control the position of the quadrotor, which allows it to reject constant disturbances.

With respect to the wind estimation, the main results are related to data coming from the wind tunnel experiments. They allowed us to perform a preliminary evaluation of the drag and lift coefficients adjusted by the area (A) of the section of the quadrotor interested by the wind flow. It was also possible to evaluate how wind speed and the pitch angle influence the thrust vector. Such aspects need further refinement and validation due to the few experiments that we were able to perform for the pitch variations.

For real flights the identification of the $c_L A$ coefficient with turning propellers would be a future work of great interest because in that case they could act as wings and could have a large influence regarding the lateral in-flow.

This work could be a starting point for other projects addressing wind estimation on quadrotors, a crucial part of its overall control structure.

The main future works, beside those described above, which can be developed starting from this work are reported below:

- Validation of the results through real flights.

- Experiments in the wind tunnel with only one motor and one propeller.

- Identification of the full aerodynamic model of the quadrotor, and also analyzing the torque equations.

REFERENCES

[1] Quentin Lindsey, Daniel Mellinger, and Vijay Kumar. Construction of cubic structures with quadrotor teams. In Hugh F. Durrant-Whyte, Nicholas Roy, and Pieter Abbeel, editors, *Robotics: Science and Systems*, 2011.

[2] J Alonso-Mora, M Schoch, A Breitenmoser, R Siegwart, and P Beardsley. Object and animation display with multiple aerial vehicles. In *Proc. of the IEEE/RSJ International Conference on Intelligent Robots and Systems (IROS)*, 2012.

[3] Caitlin Powers, Daniel Mellinger, Alex Kushleyev, Bruce Kothmann, and Vijay Kumar. Influence of aerodynamics and proximity effects in quadrotor flight. In *Proceedings of the International Symposium on Experimental Robotics*, June 2012.

[4] Rahul Goel, Sapan M. Shah, Nitin K. Gupta, and N. Ananthkrishanan. Modeling,simulation and flight testing of an autonomous quadrotor. In *ICEAE*, 2009.

[5] Konrad Rudin. Lecture Slides of the *Unmanned Aircraft Design, Modeling and Control* course: Dynamic Modeling of MAVs, 2013.

[6] Anthony RS Bramwell, David Balmford, and George Done. *Bramwell's helicopter dynamics*. Butterworth-Heinemann, 2001.

[7] Erdinc Altug, James P Ostrowski, and Robert Mahony. Control of a quadrotor helicopter using visual feedback. In *Robotics and Automation, 2002. Proceedings. ICRA'02. IEEE International Conference on*, volume 1, pages 72–77. IEEE, 2002.

[8] http://www.pixhawk.ethz.ch. Pixhawk, 2012.

[9] http://ardrone2.parrot.com/. Parrot AR drone, 2012.

[10] N. Michael, D. Mellinger, Q. Lindsey, and V. Kumar. The grasp multiple micro UAV testbed. *IEEE Robotics and Automation Magazine*, 2010.

[11] MATLAB, version 8.2 (R2013b), The MathWorks Inc., 2013, Natick, Massachussetts.

[12] Institut für fluiddinamik IFD of ETH, http://www.ifd.mavt.ethz.ch/, 2013.